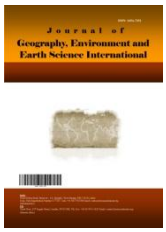

Journal of Geography, Environment and Earth Science International

26(9): 1-16, 2022; Article no.JGEESI.92287
ISSN: 2454-7352

Identification of Groundwater Bearing Zones Using Geoelectrical and Electromagnetic Techniques at Tourah Area, South of Cairo - Egypt

Fardous M. Zarif [a*]

[a] *Geophysical Exploration Department, Desert Research Center, P.O.Box-11753, El-Matariya, Cairo, Egypt.*

Author's contribution

The sole author designed, analysed, interpreted and prepared the manuscript.

Article Information

DOI: 10.9734/JGEESI/2022/v26i930369

Open Peer Review History:
This journal follows the Advanced Open Peer Review policy. Identity of the Reviewers, Editor(s) and additional Reviewers, peer review comments, different versions of the manuscript, comments of the editors, etc are available here: https://www.sdiarticle5.com/review-history/92287

Original Research Article

Received 30 July 2022
Accepted 21 September 2022
Published 26 September 2022

ABSTRACT

The complex geology of Tourah area, south Cairo is a serious challenge for groundwater exploration, where the risk of unsuccessful groundwater drilling excavation for industrial purposes is well dressed, raising the need for better geophysical subsurface detection and characterization approaches in terms of water bearing and aquitard zones. Datasets from the study area were acquired using integrated geophysical techniques comprising of one Dimensional Vertical Electrical Soundings (1D VES) and one Dimensional Transient Electromagnetic (1D TEM) as well as two-Dimensional Electrical Imaging (2D ERI) which was restricted to the available spreading space as well as subsurface infrastructure noise. The results of 1D VES and 1D TEM soundings detected three to five geoelectric layers used to generate geoelectrical cross sections and maps of resistivity, thickness, and depth to water bearing zone. Moreover, the 2D ERI inversion profiles were able to image the first three layers and the depth of the water bearing zone [A] with significantly greater resolution due to their higher lateral and vertical resolutions compared to the traditional 1D VES and TEM interpolated cross section. The integration of the three geophysical methods displayed a smooth distribution of both marly limestone and fractured shaly limestone and claystone bands water bearing zones [A and B]. Resistivity values of the water bearing zone [A] ranges from 0.1 to 24 Ω m, with average thickness of 4 to 12 m, and depth to water of 1.5 to 13.6 m. In addition, [zone B] is the main water bearing zone of fractured shaly limestone and claystone bands (2 to 14 Ω m) which is detected at deep depth of 40 and 75 m. Two normal fault systems inferred from 1D

**Corresponding author: E-mail: Fardous.drc@drc.gov.eg, Fardous.drc@gmail.com;*

interpretation are considered responsible for local recharging of the main Eocene aquifer over the study area. In conclusion, the outlined water bearing thickness as well as limited sources of groundwater recharge indicate that these water bearing zones may not provide a sustainable supply for the industrial development purposes in the future.

Keywords: Groundwater; electrical resistivity; electromagnetic; Eocene limestone: industrial development.

1. INTRODUCTION

Groundwater is an important supply of freshwater that is utilized for domestic, industrial, and agricultural uses all over the world. Groundwater usage for agricultural expansion, in instance, has increased tremendously over the last decade, particularly in highly populated countries such as South Asia, Africa, and China [1] and [2].

The study is being carried out at middle Eocene limestone southeast of Helwan, Egypt, to investigate the groundwater setting within the Tourah Cement factory. Water scarcity has always been a problem in the cement industry. As a consequence, geophysical surveys were performed to explore the issue and identify water bearing zones. Because borehole information is typically expensive, geophysical techniques for near surface geological, hydrological, and geotechnical characterization have grown rapidly during the last several decades [3]. The use of geophysical techniques to effectively explore groundwater in complex geology regions such as Tourah area demands a detailed understanding of its hydrogeological properties, particularly in arid and semi-arid environments, to increase the chance of successfully digging water wells.

This research will focus on using 1D Transient Electromagnetic (1D TEM), 1D Vertical Electrical Sounding (1D VES) and two-Dimensional Electrical Resistivity Imaging (2D ERI) methods which are commonly employed for groundwater exploration [3-10]. Geoelectrical resistivity techniques are commonly employed to explore groundwater in both porous as well as fractured rocks. When saturated with groundwater, clean sands and gravels with primary porosities always produce suitable aquifers, which may be distinguished from lower resistivity impermeable marls and clays, as well as bedrock, which is primarily of significantly higher resistivity [11]. Most Previous work in the study area or its vicinities have only focused on the causes of the Landslides articulation and water seepage to the ground surface at the quarry open pit. However, far too little attention has been paid to groundwater exploration for industrial and agricultural applications.

The geoelectrical resistivity approach is now widely used in hydrological investigations, mineral and mining exploration, as well as environmental and engineering applications [12-15]. This geoelectrical resistivity approach is regarded as one of the best geophysical methods for detecting groundwater in fractured limestone sites, mapping plumes, mapping saline groundwater boundaries, and exploring geothermal fluids. Furthermore, 1D TEM technique is considered a powerful fast and effective method for identifying high conducting zones [16-18]. Because of the strong connections between the electrical resistivity and electromagnetic and their geology and fluid content, both approaches (electrical resistivity and electromagnetic) have been frequently employed as exploratory tools in groundwater studies [9]. Thus, combining 1D TEM and direct-current (DC) resistivity techniques, both of which are sensitive to electrical conductivity, can offer information on a hydrogeological framework of a region at multiple scales [9,19,20].

1.1 Study Area

Tourah is located in the northeastern part of Egypt's Eastern Desert. The study area is located downstream of Wadi Garawi, which flows into the Nile and represents the northern basin of the Eastern Desert (Fig. 1). The surface of the study area, as well as all of the eastern and southern adjacent areas till Assuit, is primarily covered with Eocene carbonate rocks [21-27] studied the geology of the Helwan area in general and the Tourah area in particular. The geological setting of the Tourah area is mostly covered in Fig. 2: Many publications defined the stratigraphic units in southeast Cairo city as Tertiary (Middle Eocene, Upper Eocene, and Oligocene) and Quaternary (Nile deposits and alluvium deposits). Several categories for the Eocene rocks in the study area were offered (Figs. 2 & 3).

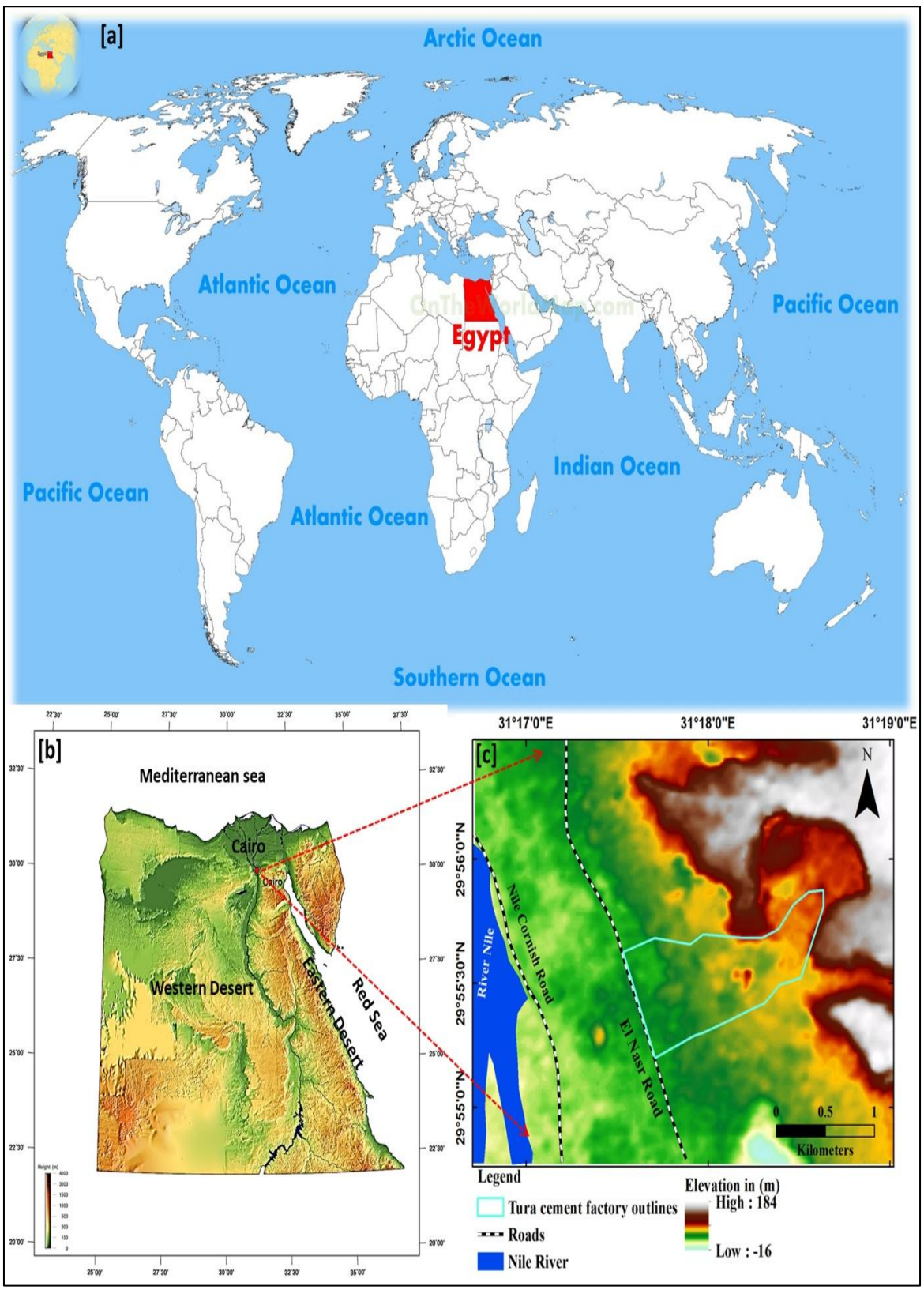

Fig. 1. [a] Egypt by the world map (https://www.whereig.com/egypt/). [b] Digital elevation map for Egypt with the location of south Cairo. [c] Location map of the investigated area, South of Cairo

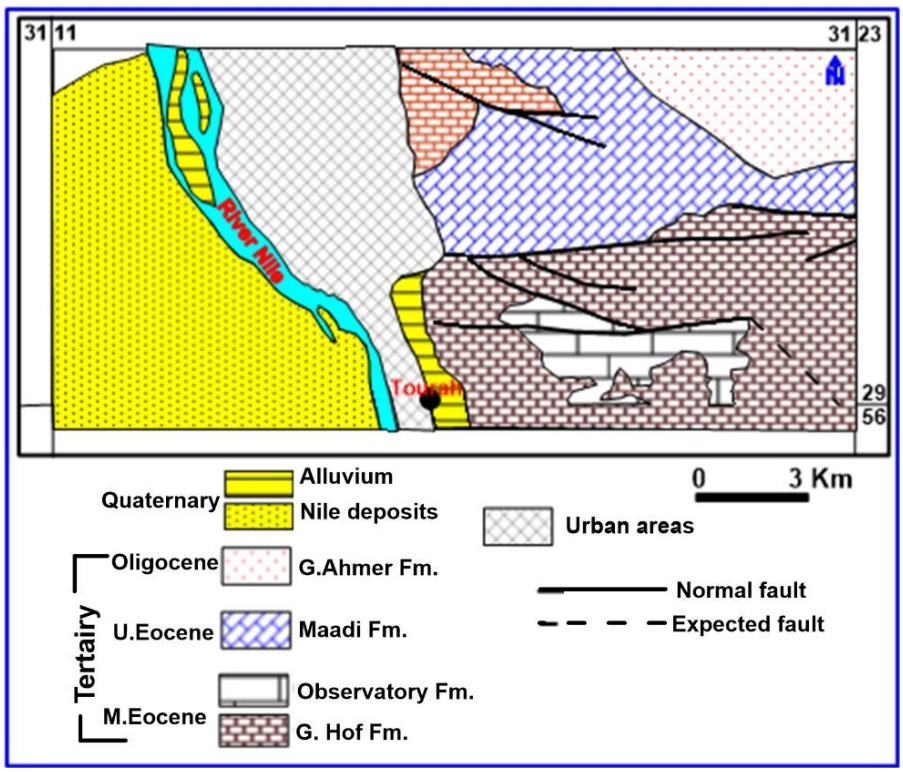

Fig. 2. Geologic map of Tourah area, simplified from the Geological Survey of Egypt and Conoco Coral (1987)

Moustafa et al. [24,28,29] defined Mokattam unit. Mokattam Formation covers the whole surface of east Helwan city (Fig. 2) and is consisting of two formations: Gebel Hof Formation at the bottom and Observatory Formation at the top. An unconformity surface separates Mokattam Formation from the overlying Maadi Formation.

Wadi Garawi and Qurn Formations represent Middle Eocene sediments, whereas the Wadi Hof Formation represents upper Eocene deposits. Wadi Garawi Formation is made up of marl and marly limestone with clay intercalation in the top section of the formation with thicknesses varying from 50 to 80 m. Qurn Formation is made up of five units, the first of which is large crystalline limestone interbedded with argillaceous limestone (as indicated in the composite geological section) (Fig. 3). The second unit consists of argillaceous limestone, marl, and shale. The third section of Qurn Formation is mostly composed of marl and shale. Limestone with claystone bands is the fourth unit. The fifth and last unit (at the top) of Qurn Formation is made up of limestone. The Middle Eocene Observatory Formation is distinguished by extensively broken limestone and caverns [25,30,31].

Structurally, the study area is mostly transected by normal faults (Fig. 3). A large number of normal faults have been discovered to the north of the Tourah cement area. Some of these faults extend for more than 10 km. It runs E-W and NW-SE direction, with the downthrown side to the north. As far as the northern section of Egypt is concerned, as documented by Said [24], the study area was mostly influenced by the following faulting and folding patterns:

a) Faulting Pattern: The area was predominantly impacted by two faulting systems: an erytherian trend that runs in a N55^{o} W direction. It mostly affects the Eocene limestone plateau. This is the younger trend, which has an effect on the older (NE) trend. Tethyan trend with an E-W axis. It affects Gebel Mokattam, Cairo-Suez Road, and Gebel Hof in the north. In general, all of the faults are of normal gravity.
b) Folding System: The area under consideration has no obvious folds. The only fold is noticeable north and south of Gebel Yahmoum El Asmr, as well as along the Maddi-Kattamiya Road, where the fold axis trends NW-SE.

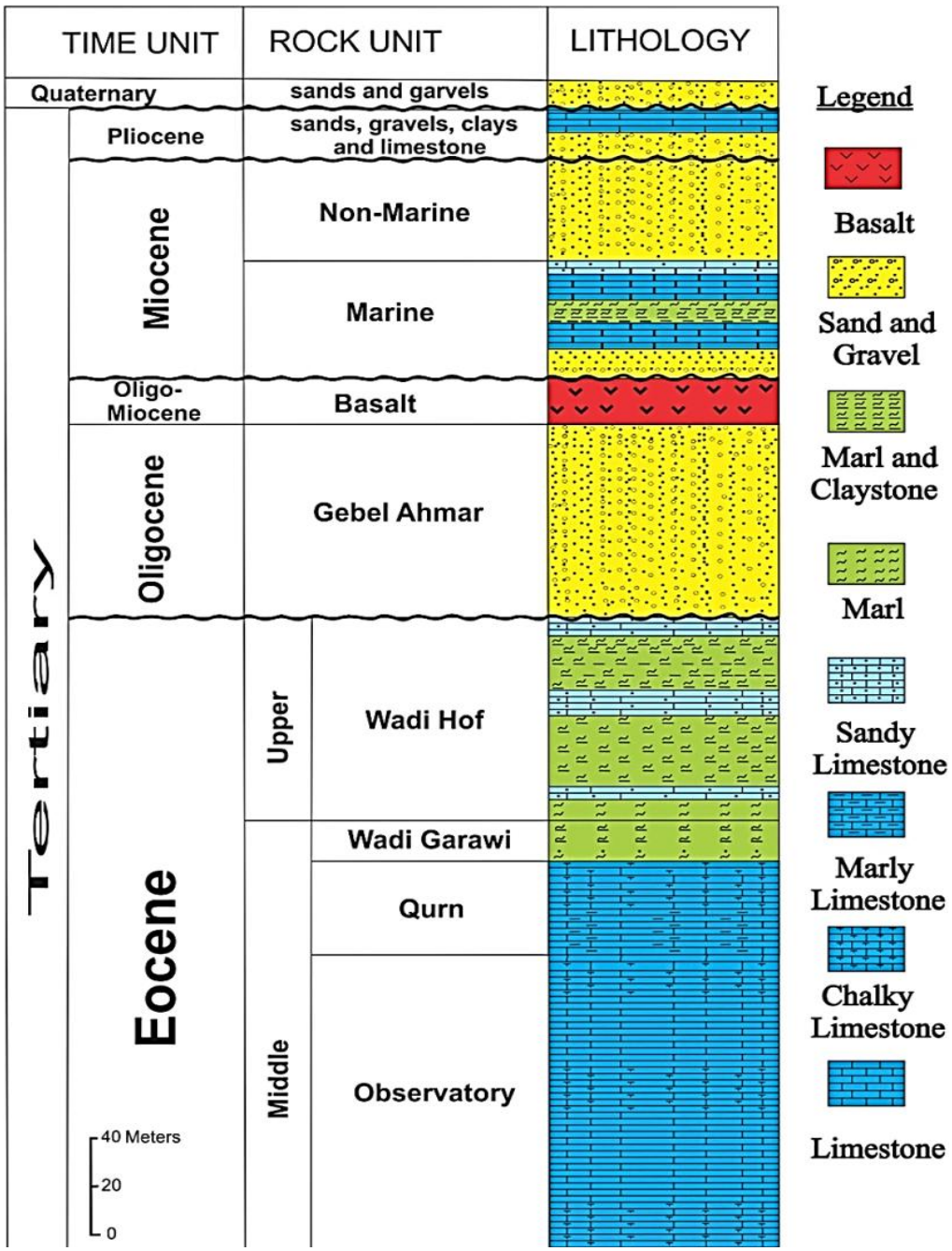

Fig. 3. Generalized stratigraphic column of the study area (simplified after Abd-allah and Moustafa, 1991 [26]

2. MATERIALS AND METHODS

1D Vertical Electrical Sounding (1D VES), 1D Transient Electromagnetic (1D TEM), and 2D-Electrical Resistivity Imaging [2D ERI] methods were all integrated in the current study to study the groundwater potentiality in the area under investigation. A total of eight (1D VES) were measured using a Schlumberger array with a maximum current electrode spacing that varies from one VES to another (from 75 m to 500 m). The 1D VES data was collected using a field instrument (ABEM Terrameter, SAS1000). 1D TEM measurements were performed at 10 study sites using a TEM-FAST 48 HPC instrument (Version 8) and a single square loop configuration (used as transmitter and receiver) with dimensions of 50 x 50 m at 7 TEM soundings, 75 x 75 m at 2 TEM soundings, and 200 x 200 m at 1 sounding, with a current

strength ranging from 1–4 A. 2D ERI profile measurements were taken at six different sites. Wenner electrodes array was used with spacing 5 m and a total length of 60 m at profiles 3 and 6; spacing of 10 m and a total length of 150 m at profiles 2,4 and 5; and spacing of 15 m with a total length 420 m at profile 1. The measurements were taken with ABEM Terrameter, SAS1000 field instrument. Fig. 4 shows the locations of the geophysical measurements.

2.1 1D Vertical Electrical Sounding (1D VES) and Transient Electromagnetic (1D TEM) methods

The 1D VES method, as demonstrated by Flores and Velasco [31,32], is sensitive to both resistive and conductive layers. However, if these layers have thin thickness, the issue of non-uniqueness or equivalence becomes severe. The 1D TEM method is less influenced by equivalence in the case of conductive layers, but it may also be less sensitive to layers with high resistivities. As a result, combining each method can result in higher subsurface layering succession results. As a consequence, the VES and TEM data were inverted, with the Tourah well (1) data set model operating as a standard or initial model to govern the inversion (Fig. 4). The 1D VES and TEM data were inverted using the IPI2 Win sounding interpretation Version 3.0.1.a7.01.03 (1990-03) and Zond TEM1D (version 5.2) software packages, respectively. These Windows Programme enables for forward and inverse modelling of 1D VES and TEM data. Fig (5a & d) shows examples of 1D VES and TEM inversion using the mentioned software packages. In April 2019, Water and environmental solution Company dug inside Tourah Cement Factory a new well (Tourah well 1), close to VES (7). The information of this new well is utilized as a starting model to calibrate the inversion of 1D VES and TEM measurements (Fig. 5b).

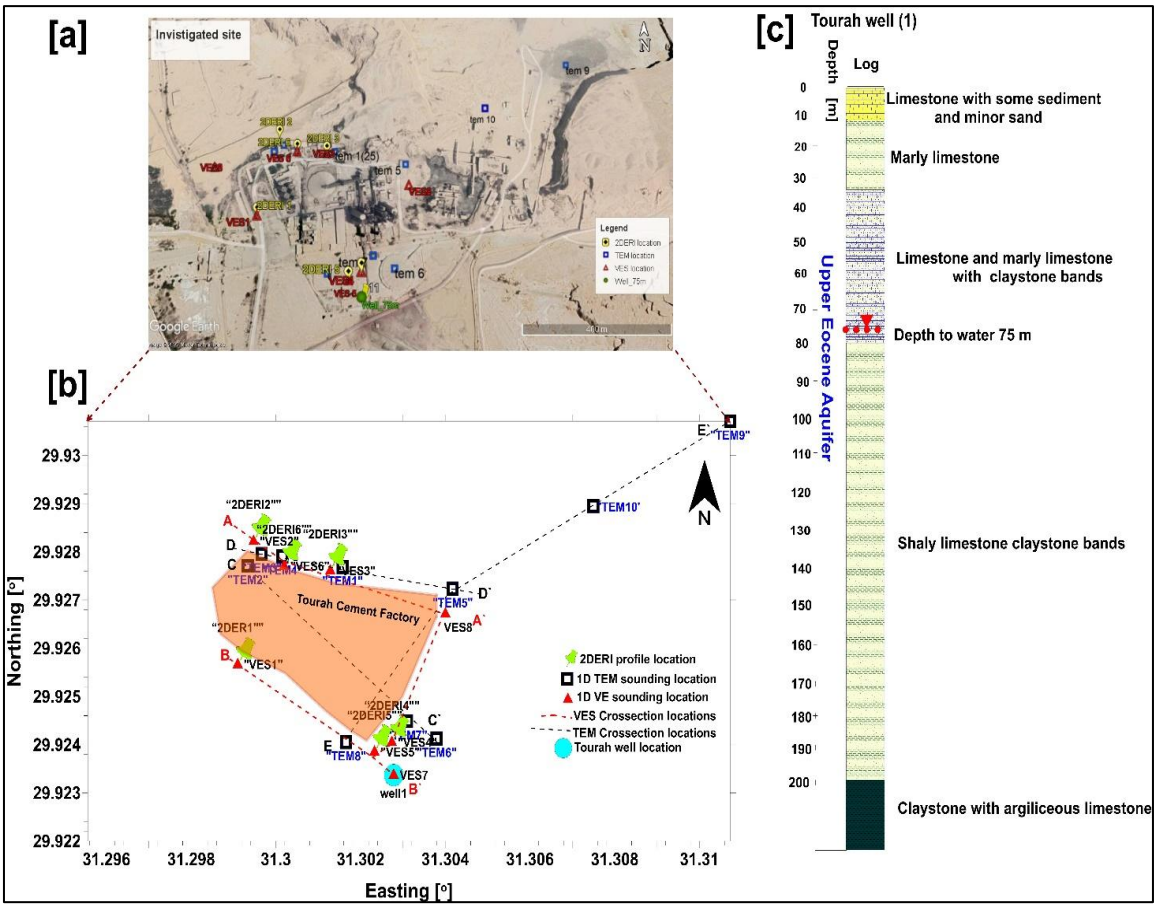

Fig. 4. [a] Field location on google earth map. [b] The locations of 1D VES, 1D TEM soundings, 2D ERI profiles. [c] The lithology description of Tourah well (1)

2.2 2D Electrical Resistivity Imaging (2D ERI) Survey

The conventional resistivity study employs four electrodes: two current and two potential electrodes. The electrodes are arranged according to the purpose of the survey. Electrical sounding provides 1D vertical information about the subsurface using the four-electrode resistivity survey [33]. With the introduction of computers into resistivity surveys, many electrodes may now be linked to multicore cables that are connected to a resistivity meter [34]. The computer (resistivity meter) has been programmed to choose combinations of four electrodes at any given time, producing a 2D data set. 2D ERI techniques provide 2D information about the subsurface layering. Equation 1 gives the apparent resistivity of subsurface materials.

$$\rho a = \frac{2\pi aV}{I} \quad (1)$$

Where ρa is the apparent resistivity (Ω m), V is the electric potential, a is distance from a point electrode and I is the electric current.

Inversion of the electrical resistivity imaging profiles was made by applying RES2DINV.EXE ver. 3.59.121 software (Geotom Software SdnBhd, 2009). It is a Windows-based computer program that automatically determines a (2D) resistivity model of the subsurface for the data obtained from electrical imaging surveys [34].

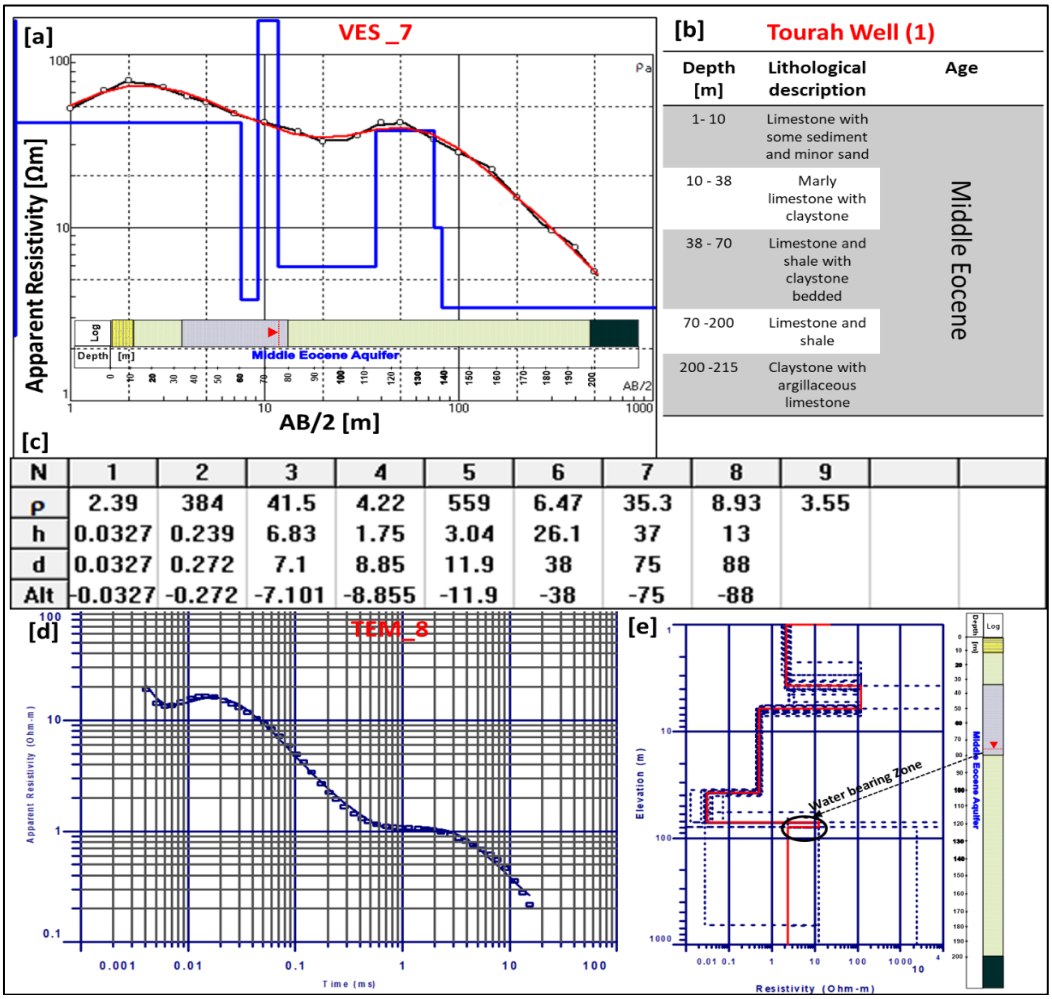

Fig. 5. Results of 1D VES and TEM soundings at the investigated site. [a] The layered model of VES no. 7 is compared with lithology of the nearby well Tourah well (1). [b] Tourah well lithology description with depth. [c] The finding of VES no.7 inversion. [d] The layered model of TEM sounding no. 8 and [e] The model layers of TEM no. 8 compared with lithology of Tourah well (1)

3. RESULTS AND DISCUSSION

3.1 1D Vertical Electrical sounding (1D VES) and 1D transient Electromagnetic (1DTEM) Methods

Results of both 1D VES and TEM soundings showed the division of the subsurface layers into three to five layers according to their geoelectrical properties. Tourah Well (1) (Fig. 4) data of drilled well greatly helped in setting the initial model of building the interpretation model. There is a near agreement between the interpretations resulting from the data of 1D VES and TEM soundings. The main difference between the two methods is 1D TEM is more sensitive to conductive bodies than 1D VES method. Here, in this study, the 1D VES measurements couldn't reach depths of more than 14 m except at VES 7, where the maximum depth is 88 m where AB/2 reaches 500 m and this can explain why that layer number of TEM measurements is more where loop size ranges between 25×25 m and 200×200 m.

The findings of the geoelectrical interpretation for 1D VES and TEM soundings (VES 7 and TEM 8) measured nearby Tourah Well (1) reveal an agreeable resemblance for the outcomes of the water well data (Fig. 6b) and (Fig. 7c). An example of the correlation between the interpretation of TEM (8) and VES (7) and the lithological description for the Tourah well (1) is shown in Fig. (5a & e). The results of the geoelectrical interpretation were used to construct the subsurface cross sections that comprises different geoelectrical layers. Two cross sections (A-A` and B-B`) illustrated in Fig. (6 a & b) from VESes interpretation that run in NW-SE direction, and three cross sections (C-C`, D-D` and E-E`) from TEM interpretation run also in NW-SE direction except cross section E-E` which is oriented in NE-SW direction. The first geoelectrical layer (L 1) is characterized by relatively moderate to high resistivity values ranged between 83 Ω m (VES 6) along A-A` cross section and 560 Ω m (VES 7). The thickness of this layer is ranged between 1.5 m (VES 2) and 21 m (VES 1), which corresponds to the surface limestone, rock sediments and minor sand. The second geoelectrical layer (L 2) is characterized by relatively moderate to low resistivity values ranged between 4 Ω m (VES 8) and 24 Ω m (VES 1). The thickness of this layer is ranged between 4 m (VES 3) to about 12 m (VES 7) which corresponds to the water bearing marly limestone layer [zone A]. The third geoelectrical layer (L 3) is characterized by a varied resistivity value ranging between 2 Ω m (VES 3) and 69 Ω m (VES 7) which corresponds to limestone and shale which changed laterally to clay sediments under VES 3 and VES 6 which is considered the last layer along cross section A-A`. Otherwise, along cross section B-B` (Fig. 6b) the geoelectrical layer (L 4 and L5) are detected under VES (7). Geoelectrical L 4 is considered the main water bearing zone [B]. This layer is formed of fractured shaly limestone is located at depth 75 m based on the drilled information of Tourah Well (1). The estimated resistivity value of this zone is 9 Ω m with thickness of no more than 20 m. L 5 is the last geoelectrical layer under VES (7) and is composed of claystone and its lower surface is not detected at the rest of measured 1D VES soundings (Fig. 6).

On the other hand, 1D TEM interpretation offers more deeper in subsurface details than 1D VES method, which is constrained by the limited spreading inside and around the cement factory (area under investigation). The first three geoelectrical layers (L 1, L 2 and L 3) are in agreement with 1D VES results except some changes in resistivity values results of L 2 and L 3 in 1D TEM results, where they are classified as low to very low resistivity due to the facies changes from marly limestone to shale and claystone bands. Along cross sections C-C`, D-D` and E-E` (Fig. 7a, b & c), the first geoelectrical layer [L 1] is represented by the uppermost part of the dry zone; it has resistivity values range from 89 Ω m at TEM 8 to 1521 Ω m at TEM 5. The variations in resistivity values are due to the variations in the exposed sediments on the ground surface that vary from fine sediments (sand) to compacted limestone derived from the northeastern plateau. The thickness of this layer varies from 2 m at TEM 9 to 6.3 m at TEM 4. The second geoelectric layer [L 2] has resistivity values range from 0.1 Ω m at TEM 10 to 7.8 Ω m at TEM 4; and its thickness varies from 2.2 m at TEM 7 to 26 m at TEM 2. It is correlated with the intercalated marly limestone with claystone bands. As previously clarified in VESes cross sections, this layer is considered the first water bearing zone [A].

The third geoelectric layer [L 3] represents claystone. Its resistivity values range from 0.1 Ω m at TEM 1 to 8 Ω m at TEM 9 and thickness varies from 14 m at TEM 1 to 60 m at TEM 9, it gets thinner toward the southwest directions.

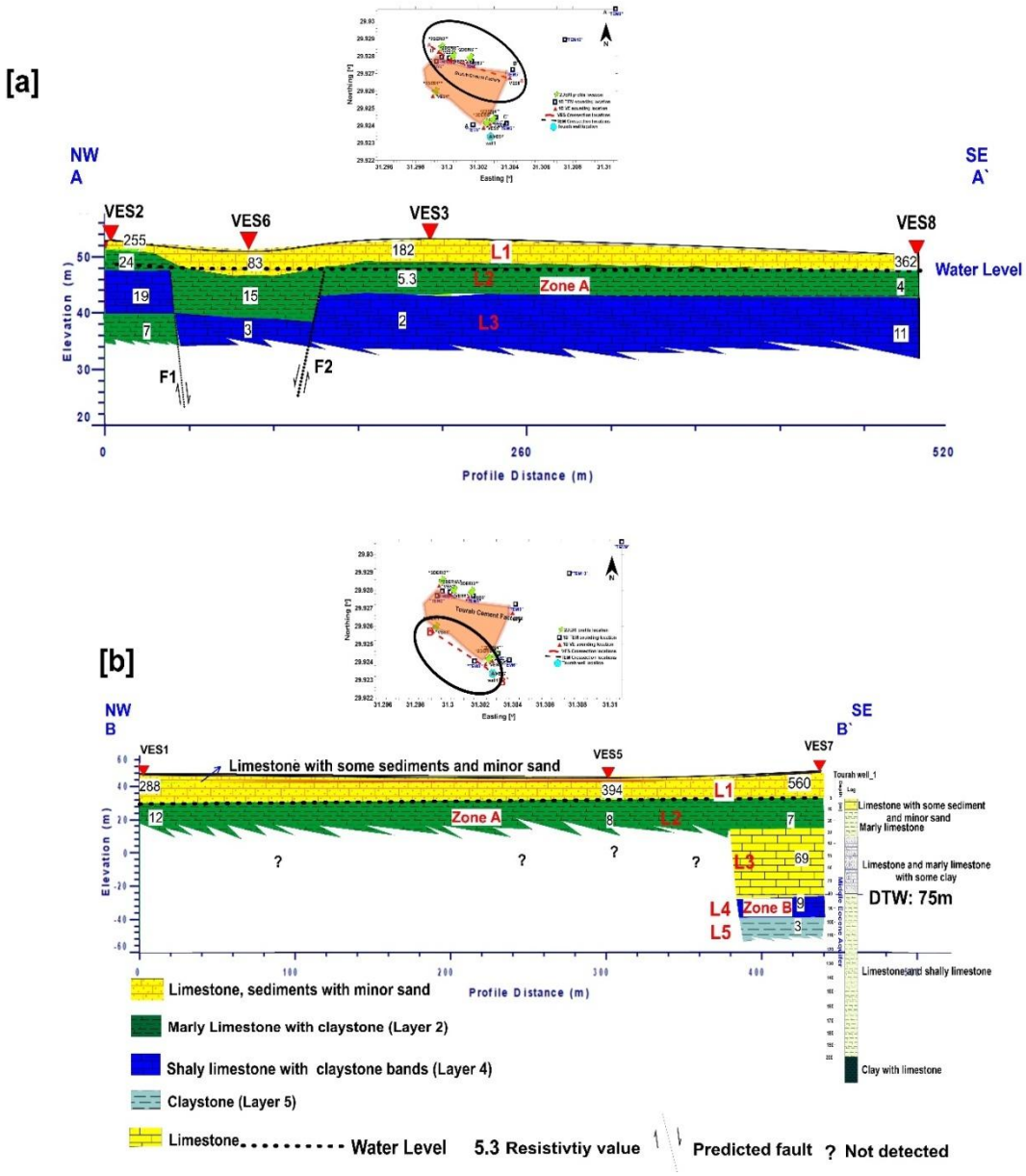

Fig. 6. Geoelectrical cross sections in NW- SE direction inferred from the interpretation of 1D VES soundings measurements with the lithological of Tourah well (1). [a] Geoelectrical cross section A-A`. [b] Geoelectrical cross section B-B`

The fourth geoelectric layer [L 4] is the most important layer in this succession; it represents the water bearing zone [B] of fractured shaly limestone with banded of claystone. Its resistivity values range from 2 Ω m to 14 Ω m at TEM1 and TEM 9 respectively and its thickness varies from 15 m at TEM 2 to 35 m along cross sections D-D` and E-E` respectively (Fig. 7b & c); the thickness of this layer was not detected at TEM 1, TEM 3, TEM 4 and TEM 8 along D-D` cross section.

The lower resistivity values of this zone can be attributed to the increase in the water salinity and/or the increase in the clay content. This layer rest over the fifth layer [L5], which is described as an impervious layer (clay bed) and considered the base of the upper Eocene aquifer with resistivity range from 0.15 Ω m at TEM 10 to 6 Ω m at TEM 9 along cross section E-E` (Fig. 7c); and its lower boundary was not detected under the measurable TEM soundings.

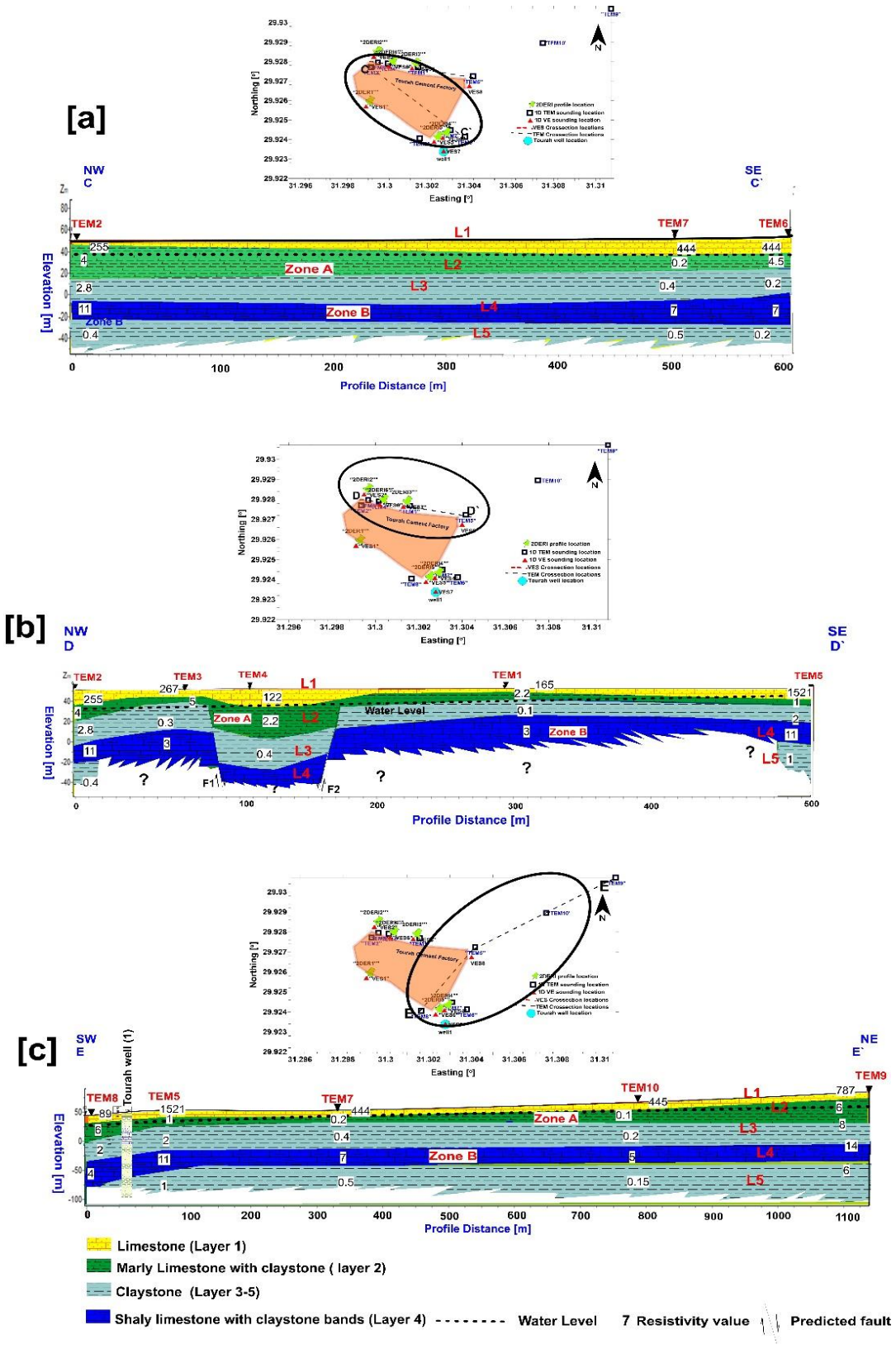

Fig. 7. Geoelectrical cross sections inferred from the interpretation of 1D TEM measurements. [a] C -C` cross section in NW-SE. [b] D-D` cross section in NW-SE and [c] E-E` cross section in SW-NE direction. L1 (layer 1), L 2 (layer 2), L 3 (layer 3), L 4 (layer 4) and L 5 (layer 5)

In order to clarify the characteristic properties of the water bearing zones in the area under investigation, six maps were constructed (Iso resistivity map, Isopach map, and depth to the water bearing zones maps). The Iso resistivity maps (Fig. 8a & b) show that; the resistivity values of the water bearing zone [A] tend to be increased toward the west direction, whereas the value decrease towards the northeastern direction. This layer is considered the shallow water bearing zone [A] with very low resistivity (0.1 -7.8 Ω m). This zone mainly composed of marly limestone interbedded with claystone layers. The low resistivity may be related to the source of the recharge which drains from the seepage of irrigation agricultural lands in the west of Nile valley and industrial cement wastewater. On the other hand, the resistivity of second water bearing zone [B] is increasing towards the northeast direction and vice versa in the west and southwest direction where the drilled well (Tourah well1) is located. The resistivity decreases to around 3 Ω m with poor water quality [Total Salinity~ 7000 ppm). The isopach maps (Fig. 8c & d) indicate that the saturated thickness of water bearing zone [A] increases in northeast and west direction where, the water bearing zone [B], which is considered the main Middle Eocene aquifer (Qurn Formation) in the study area, its thickness increases in general toward the northeastern side of the study area and decreases in west and southwest direction where Cement factory is located. The top surface of water bearing zone [A] is located at depths range between 1.6 m and 13 m where, the main water bearing zone [B] is located at depths varying from 40 m to more than 75 m (Fig. 8e & f). Regionally, it increases towards the northeastern part of the study area due to the increase in the ground elevation. According to the findings of this study, the priority of groundwater occurrences and exploitations in the area under investigation typically depends mainly on Zone [B] which increases toward the northeastern part, where Wadi Garawi and Qurn Formation of Middle Eocene Aquifers occupies this part (Eocene plateau). The optimum places to use the groundwater shaly limestone with claystone bands of the Middle Eocene age lie in the northeastern and eastern regions of the research area. The water bearing thickness and groundwater recharge sources indicate that this zone may not provide a sustainable supply for industrial development needs. Moreover, the groundwater quality/salinity (~7000 ppm) suggests that specific treatments are required to make this water suitable for consumption purposes.

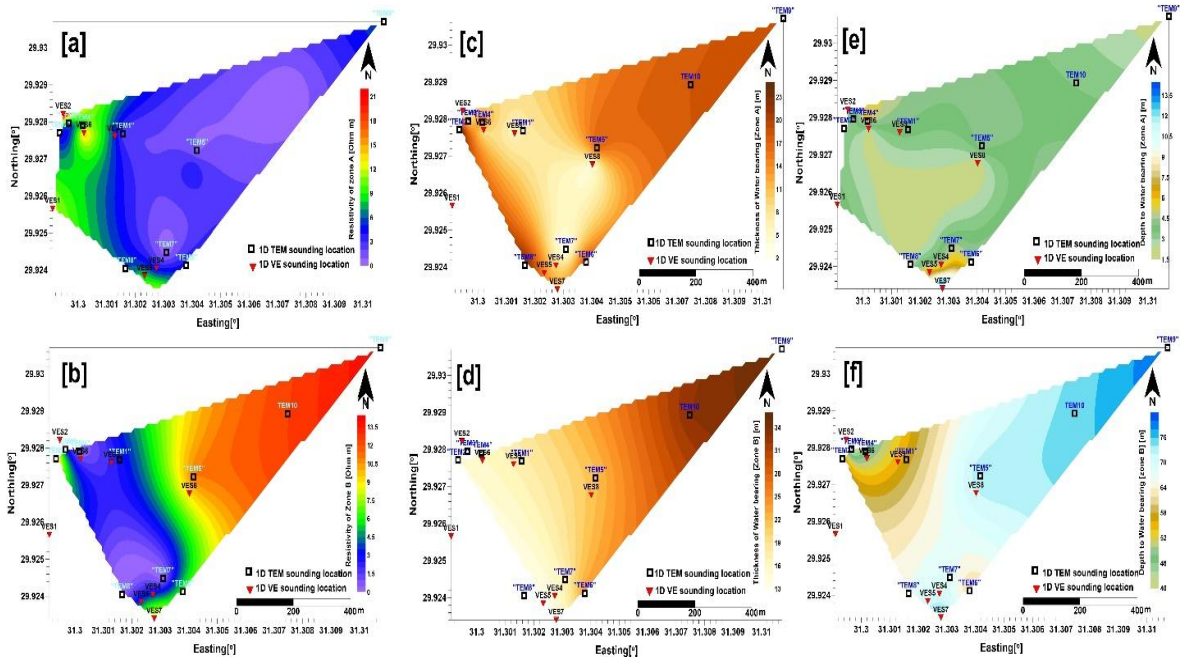

Fig. 8. Iso resistivity contour maps for [a] water bearing of zones A and [b] for water bearing zone B. [c] Isopach contour maps for water bearing of zones A and [d] for water bearing zone B. [e] Depth to top of water bearing zone A where [f] Depth to water bearing zone B in the area under investigation

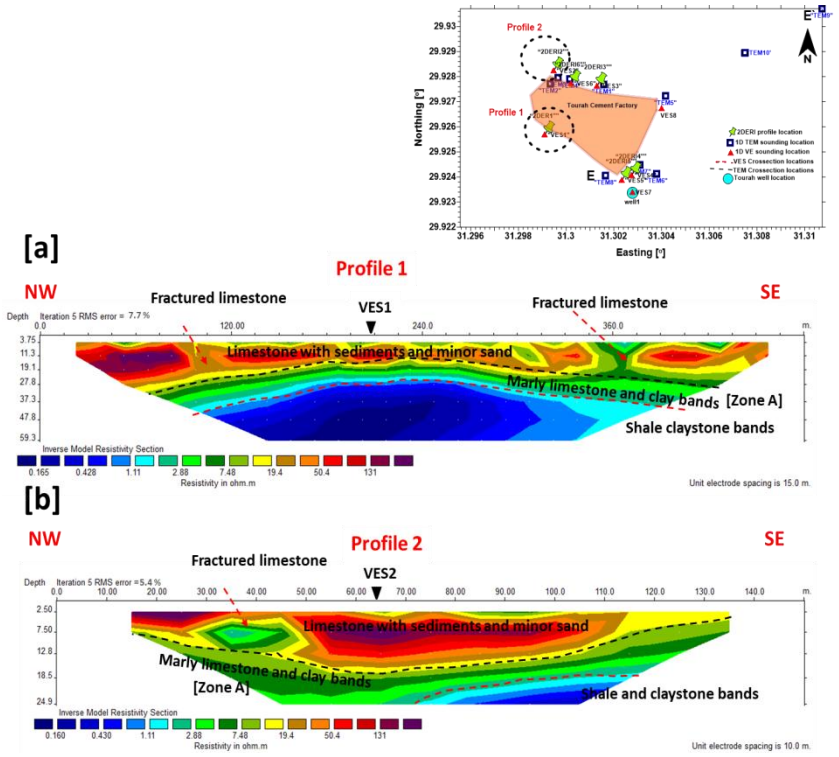

Fig. 9. 2D inversion results of 2D ERI. [a] Profile 1. [b] profile 2 in NW-SE direction

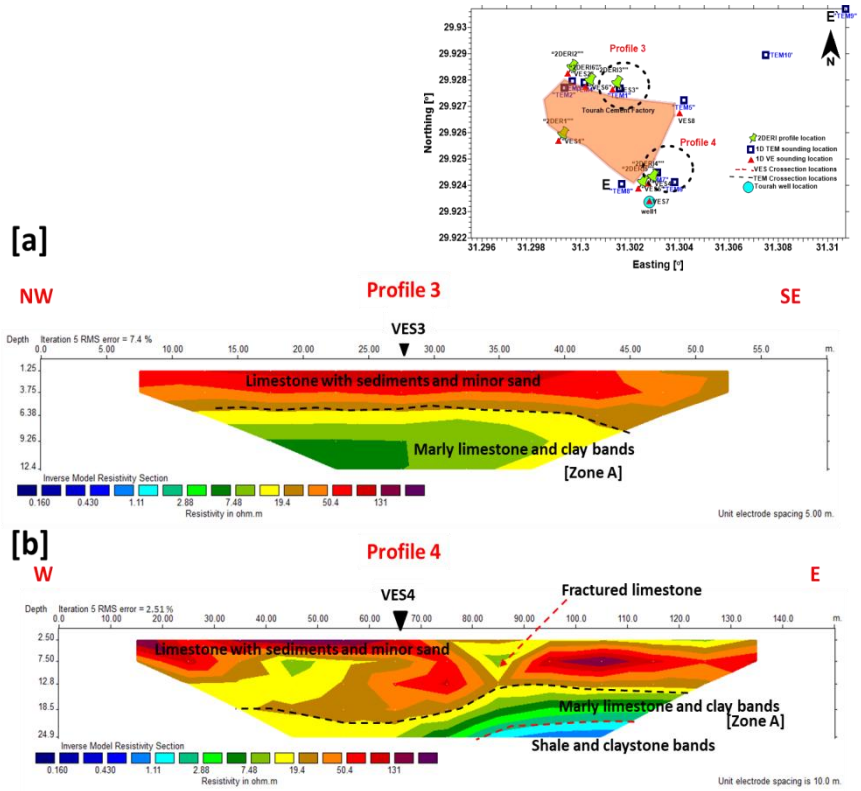

Fig. 10. 2D inversion results of 2D ERI. [a] Profile 3 in NW- SE direction[b] profile 4 in W - E direction

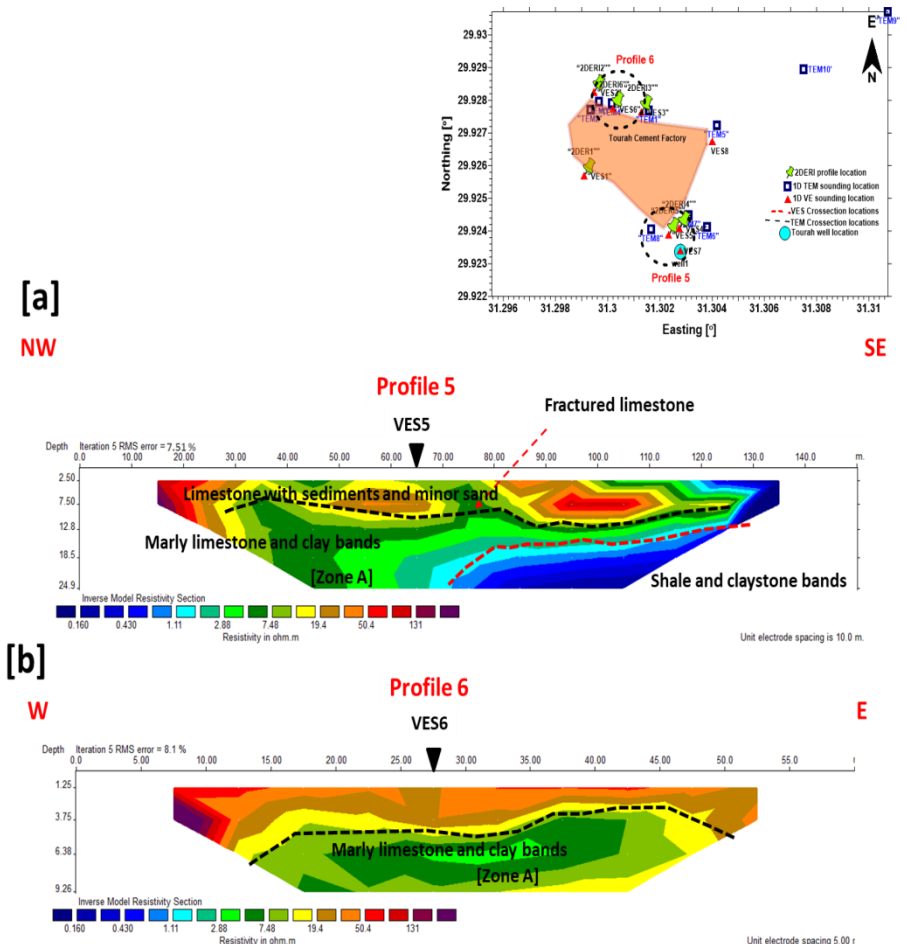

Fig. 11. 2D inversion results of 2D ERI. [a] Profile 5 in NW-SE [b] profile 6 in W - E direction

The area under investigation has been transected by two normal faults F1 and F2 inferred from the both 1D VES and TEM interpretation. These faults are responsible for enhancing the storage of the aquifers.

3.2 2D Electrical resistivity imaging [2D ERI] survey

2D ERI data are inverted using software Res2Dinv of (Loke, V.3.7, 2015). The six profiles exhibit three main geoelectric layers. These layers are in agreement with the first three layers obtained from results of 1D VES and TEM soundings. The first layer (L 1) shows a homogeneous resistive superficial layer of limestone with resistivity ranges between 50 and 131 Ω m. This thickness of this layer is varying at the six profiles sites. It ranges from 6.3 m at profile 6 to 19 m at the middle part of profile 1 and decreases to be 4 m at profile 6 (Fig. 11b) and increase in the both side of profile 1 to be 37 m. Some profiles, such as profiles 1, 4, and 5, have an abrupt due to fractured filled with resistive materials/clay. A thin layer of low to moderate resistivity ranges from 1.1 to 7.8 Ω m and a thickness of no more than 20 m is found below [L 1]. This layer [L 2] is considered the shallow water bearing zone [A] and mainly composed of marly limestone with claystone bands. This layer is located at different depths at the 6 sites of the profiles (19 m at profile 1, 12 m at profile 2 (Fig. 9b), and the rest of profiles nos. 3,4,5 and 6 it located at 6.3 m, 7.6 m, 8 m and 4 respectively (Figs. 10a & b and 11a & b). The low to very low resistivity values may be corresponding to the recharge source in the area under investigation (seepage of western irrigation agricultural lands and industrial wastewater of cement factory) as mentioned before. The third geoelectric layer [L 3] has very low resistivity values (0.16 to 1.1 Ω m) which is mostly composed of shale intercalated with claystone layers. This layer appeared at profile 1 at a depth of 28 m and extended vertically to 59 m (Fig. 9a). In addition, it appears only at the southwestern

side of profile (2) (Fig. 9b) and eastern side of profile 4 (Fig. 10b), while doesn't appear at all along both profiles 3 & 6 (Figs. 10 a & 11b) moreover, the water bearing zone [B] also doesn't appear along the six profiles. The appearance and disappearance of layer from one profile to another is mainly related to the complex geology of the study area. In addition, the maximum depth of profiles 3 and 6 is 12.4 m and 9 m respectively, while, as mentioned before, this layer appears at depths ranging between 15 m and 28 m. As illustrated at Fig. (1); the limited available length for profile spreading reduced the resultant depth of penetration. Indeed, the estimated resistivity values which ranges from 0.16 to 1.1 Ω m may be related to salt water concentration with highly clay content. Black dashed line represents the interface between high resistive zone and conductive one.

The 2D ERI profiles were able to image the depth of the water bearing zone with significantly greater resolution due to their higher lateral and vertical resolutions compared to the traditional 1D VES and TEM interpolated cross section. The high-resolution 2D ERI profiles successfully imaged the thickness of the limestone layer that overlies the water bearing marly limestone with claystone bands., as well as a low resistivity vertical zone phenomime that connects the water bearing zone to near surface layer (Fig. 9a, Fig. 10b and Fig. 11a). This zone was interpreted as a local disintegration of the limestone layer, which was filled with finer sediments. The finer sediments functioned as a hydrological conduit, allowing water to rise from the deep saturated zone to the near surface layer and these results in agreement with results of Abdel Gawad, [35].

4. CONCLUSION

Both electrical resistivity and 1D transient electromagnetic methods were applied in this study in order to provide quantitative insights into the groundwater potential conditions in the area under investigation. Although Geoelectric measurements (1D VES and 2D ERI) usually can be performed in low or high electrical power density vicinities, and don't influence directly by infrastructure, but still the limited available spaces in such overcrowded environment dramatically reduced the resultant depth of investigations. On the other hand, just a few meters away from direct noise sources, 1D TEM method managed to provide useful information in such sites with reasonable probe depth around structures with metal roofs and walls compared to geoelectric measurements and TEM-derived resistivity profiles, as well as 2D ERI inverted models, were combined with constrained local Tourah well (1) lithologic data to create conceptual frameworks of the local groundwater systems. The models of electrical resistivity techniques 1D VES and 2D ERI were successfully used to identify the boundary of shallow water bearing [Zone A] due to the difficulty for spreading inside cement factory, where the model of 1D TEM method was successfully used to identify the both shallow and deep-water bearing zones [A and B] of the aquifer thickness as well as groundwater potentiality. The waterbearing zones [A and B] may not offer a sustainable supply for industrial development purposes in the future. Moreover, the groundwater quality test revealed that specific treatments are required to make this water acceptable for consumption in industrial communities, and this is an important issue for future research.

COMPETING INTERESTS

Author has declared that no competing interests exist.

REFERENCES

1. Shah T, Villholth KG, Burke JJ. Groundwater Use in Agriculture: A Global Assessment of Scale and Significance for Food, Livelihoods and Nature. Comprehensive Assessment, IWMI, International Water Management Institute; 2006.
2. Giordano M, Villholth KG. The agricultural groundwater revolution: opportunities and threats to development. International Water Management Institute Colombo, Sri Lanka. 2007;420.
3. Abd El-Gawad, A. Water Seepage Source at the Extension of Tourah Clay Quarry, Southeastern Cairo Based on Geological and Geoelectrical Resistivity Measurements. Earth Sciences. 2020;9(3):108. https://doi.org/10.11648/j.earth.0903.13.
4. Frohlich R, Urich D, Fuller J, O'Reilly M. Use of geoelectrical methods in groundwater pollution surveys in a coastal environment. J. Appl. Geophys. 1994;32:139–154.
5. Louis I, Louis F, Grambas A. Exploring for favorable groundwater conditions in hard rock environments by resistivity imaging

methods: synthetic simulation approach and case study example. J. Electr. Electron. Eng., Special issue on International Conference on Earth Sciences and Electronics-2002(ICESE-2002) (http://www.geophysicsonline.gr/paper-10.pdf).

6. Bowling J, Harry D, Rodriguez A, Zheng C. Integrated geophysical and geological investigation of a heterogeneous fluvial aquifer in Columbus Mississippi. J. Appl. Geophys. 2007;62:58–73.
7. Soupios P, Kalisperi D, Kanta A, Kouli M, Barsukov P, Vallianatos F. Coastal aquifer assessment based on geological and geophysical survey, North Western Crete, Greece. Environ. Earth Sci. 2009;61:63–77.DOI: 10.1007/s12665-009-0320-1.
8. Mesbah HS, Ismail A, Taha AI, Massoud U, Soilman MM. Electrical and electromagnetic surveys to locate possible causes of water seepage to ground surface at a quarry open pit near Helwan city, Egypt. Arabian Journal of Geosciences. 2017;10(10). Available: https://doi.org/10.1007/s12517-017-2997-x.
9. Zarif, Fardous M, Ahmed M. Elshenawy, Mohamed A. Mabrouk. Integrated TEM and 2D ERI techniques to delineate groundwater bearing zones in fractured carbonate rocks at the upstream portion of wadi Halazeen, Northwestern Coast, Egypt. Journal of African Earth Sciences. 2021;182:104288.
10. Zarif, Fardous M, Ahmed M. Elshenawy, Mostafa SM Barseem, Abdalla A. Al- Abaseiry & Ahmed N. El Sayed. "Evidence of geoelectrical resistivity values on groundwater conditions in Wadi El Natrun and its vicinities, West Delta, Egypt (cases studies). Scientific Reports. 2022;12(1): 1-16.
11. Sharma PV. Environmental and Engineering Geophysics. Cambridge University Press. Shea, PF, Luthin JN. An investigation of the use of the four-electrode probe for measuring soil salinity in situ. Soil Sci. 1997;92:331–339.
12. Griffths DH, Turnbull J, Olayinka A.I. Two-Dimensional Resistivity Mapping with a Complex Controlled Array. First Break. 1990;8:121-129.
13. Griffiths DH, Barker RD. Two- dimensional resistivity imaging and modeling in areas of complex geology. Jour. of applied Geoph., 29, Elsevier Science Publishers, B.V., Amsterdam. 1993;211-226.
14. Dahlin T, Zhou B. A numerical comparison of 2D resistivity imaging with 10 electrode arrays. Geophysical Prospecting. 2004;52: 379-398.
15. Aizebeokhai AP. 2D and 3D Geoelectrical resistivity imaging: Theory and field design. Scientific Research and Essays. 2010;5(23):3592-3605.
16. Telford WM, Geldart LP, Sheriff RE. Applied Geophysics (second edition). Cambridge University Press; 1990.
17. Gonçalves R, Farzamian M, Monteiro Santos FA, Represas P, Mota Gomes A, Lobo de Pina, AF, Almeida EP. Application of Time-Domain Electromagnetic Method in Investigating Saltwater Intrusion of Santiago Island (Cape Verde). Pure and Applied Geophysics. 2017;174(11):4171–4182.
Available: https://doi.org/10.1007/s00024-017-1642-7.
18. Kalisperi D, Kouli M, Vallianatos F, Soupios P, Kershaw S, Lydakis-Simantiris N. A transient electromagnetic (TEM) method survey in north-central coast of crete, Greece: Evidence of seawater intrusion. Geosciences (Switzerland). 2018;8(4).
Available:https://doi.org/10.3390/geosciences8040107.
19. Benson KB, Payne KL, Stubben MA. Mapping groundwater contamination using dc resistivity and VLF geophysical methods e a case study. Geophysics. 1997;62(1):80e86.
20. Bernard J, Valla P. Groundwater exploration in fissured media with electrical and VLF methods. Geoexploration. 1991; 27:81e91.
21. Awad GH, Faris MI, Abbass HL. Contribution to the stratigraphy of the Mokattam area east of Cairo" Bull. Inst. Desert Egypte. 1953;3(2):106-107.
22. Shukri NM. The geology of the desert east of Cairo" Bull. Inst. Desert Egypte. 1953; 3(2):89-105.
23. Said R. The geology of Egypt. Elsevier, Amsterdam Pub. Co., 1962;377.
24. Moustafa AR, Yehia MA, Abdel TS. Structural setting of the area east of Cairo, Maadi, and Helwan. Middle East Research Center, Ain Shams Univ. Earth Sci Ser., 1985;5:40–64.

25. Strougo A. Decouverte d'une discontinuite de sedimentation dans l' Eocene superieur du Gebel Mokattam (Egypte). C. R. Somm. Se´anc. Social Geology, France. 1976;5: 213–215.
26. Abd-allah A Moustafa. Structural setting of the central part of Cairo- Suez district. M.E.R.C., Ain Shams Univ. Earth Sc. Ser. 1991;5:133–145.
27. Zittel KA. Bitrage Zur Geology und Palontologie de libyschen wuste un angrenzenden Gebiete von Egypten. Paleontographica. 1883;30: 147. Kassel.
28. Barakat MG, Aboul Ela NM. Microfacies and paleoecology of Middle Eocene and younger sediments in geneifa area Cairo-Suez district, Egypt. J. Geol. Cairo. 1970;14(1):23-34.
29. Farag I, Ismail MM. A contribution to the structure of the area east of Helwan. Egypt. Egypt. J. Geol. 1959;3:71–86.
30. Mohamed AME, Sultan SA, Mahmoud NI. Delineation of near-surface structure in the southern part of 15th of May City, Cairo, Egypt Using geological, geophysical and geotechnical techniques. Pure Appl. Geophys. 2012;169:1641–1654.
Available:http://dx.doi.org/10.1007/s00024-011-0415-y.
31. Flores C, Velasco N. A comparative analysis between transient electromagnetic soundings and resistivity soundings in the Tres Virgenes geothermal zone, Mexico. Geofísica International. 1998;37 (3):183-199.
32. Owen RJ, Gwavara O, Gwaze P. multi-electrode resistivity survey for groundwater exploration in the Harare greenstone belt, Zimbabwe, Hydrogeology Journal. 2005; 14:244-252.
33. Dahlin T. "2D Resistivity Surveying for Environmental and Engineering Applications," First Break. 1996;14:275–283.
34. Loke MH, Chambers JE, Rucker DF, Kuras O, Wilkinson PB. Recent developments in the direct-current geoelectrical imaging method, Journal of Applied Geophysics; 2013.
DOI: 10.1016/j.jappgeo.2013.02.017.
35. Abd El-Gawad A. Landslides articulation in Wadi Hof area southeast of Cairo, Egypt, based on geological and geophysical investigations. Environmental Earth Sciences. 2021;80(5):1–12.
Available: https://doi.org/10.1007/s12665-021-09478-w.

Peer-review history:
The peer review history for this paper can be accessed here:
https://www.sdiarticle5.com/review-history/92287